Multi-Dot Floating-Gates for Nonvolatile Semiconductor Memories – Their Ion Beam Synthesis and Morphology

T. Müller,[1,*] C. Bonafos,[2] K.-H. Heinig,[1] M. Tencé,[3] H. Coffin,[2] N. Cherkashin,[2,†]
G. Ben Assayag,[2] S. Schamm,[2] G. Zanchi,[2] C. Colliex,[3] W. Möller,[1] and A. Claverie[2]

[1]*Research Center Rossendorf, Institute of Ion Beam Physics and Materials Research, PO Box 51 01 19, 01314 Dresden, Germany*
[2]*nMat Group, CNRS/CEMES, 29 Rue Jeanne Marvig, 31055 Toulouse, France*
[3]*Laboratoire de Physique des Solides, Université Paris-Sud - UMR 8502, 91405 Orsay, France*

(Dated: accepted APL draft, 4^{th} Version, February 2, 2008)

Scalability and performance of current flash memories can be improved substantially by replacing the floating poly-Si gate by a layer of Si dots. This multi-dot layer can be fabricated CMOS-compatibly in very thin gate oxide by ion beam synthesis (IBS). Here, we present both experimental and theoretical studies on IBS of multi-dot layers consisting of Si nanocrystals (NCs). The NCs are produced by ultra low energy Si^+ ion implantation, which causes a high Si supersaturation in the shallow implantation region. During post-implantation annealing, this supersaturation leads to phase separation of the excess Si from the SiO_2. Till now, the study of this phase separation process suffered from the weak Z contrast between Si and SiO_2 in Transmission Electron Microscopy (TEM). Here, this imaging problem is resolved by mapping Si plasmon losses with a Scanning Transmission Electron Microscopy equipped with a parallel Electron Energy Loss Spectroscopy system (PEELS-STEM). Additionally, kinetic lattice Monte Carlo simulations of Si phase separation have been performed and compared with the experimental Si plasmon maps. It has been predicted theoretically that the morphology of the multi-dot Si floating-gate changes with increasing ion fluence from isolated, spherical NCs to percolated spinodal Si pattern. These patterns agree remarkably with PEELS-STEM images. However, the predicted fluence for spinodal patterns is lower than the experimental one. Because oxidants of the ambient atmosphere penetrate into the as-implanted SiO_2, a substantial fraction of the implanted Si might be lost due to oxidation.

Metal-Oxide-Silicon Field-Effect-Transistors (MOSFETs) with an electrically isolated ("floating") gate layer embedded in the gate oxide are currently used as flash memories. The replacement of this floating-gate by a layer of discrete Si nanocrystals (NCs) [1] improves the performance of flash memories substantially [2]. The reduced probability for a complete discharging of the multi-dot floating-gate by oxide defects allows thinner tunnel oxides. In turn, the floating-gate will be charged/discharged by quantum mechanical direct electron tunneling (instead of defect-generating Fowler-Nordheim tunneling). The memory operation voltage can be reduced and scalability is improved. Using ion beam synthesis, the multi-dot floating-gate can be fabricated along with standard CMOS processing [3]. Si^+ ions are implanted at ultra low energies into the gate oxide, causing there a high Si supersaturation. During post-implantation annealing, this Si supersaturation leads to phase separation of elemental Si from SiO_2 [4]. Imaging this phase separation process is difficult. Till now, Transmission Electron Microscopy (TEM) has suffered from weak Z contrast between Si and SiO_2 phases. Recently, this problem was partially overcome by Fresnel imaging using under-focused bright field conditions [5]. Thus, the distance of the layer of phase separated Si from the transistor channel could be determined [6, 7]. However, this technique fails to resolve the morphology of the phase separated Si. For instance, recent kinetic Monte Carlo (KMC) simulations of phase separation predict a pronounced fluence dependence of the precipitate morphology [4]. For low Si^+ fluences, spherical and isolated Si NCs form by nucleation and growth, while for higher Si^+ fluences spinodal decomposition occurs. The elongated, non-spherical Si structures, formed by spinodal decomposition, coalesce at even higher fluences to an interconnected, labyrinthine Si network. Here, using a Scanning TEM (STEM) with an efficient parallel Electron Energy Loss Spectroscopy (PEELS) system, the predictions of KMC simulations are confirmed for the first time. The contrast problem of conventional TEM could be overcome by mapping Si plasmon losses, which differ from SiO_2. Comprehensive KMC studies and PEELS-STEM analysis has been performed to understand the complex process of phase separation in a thin buried layer.

To form Si NCs by phase separation, Si^+ ions have been implanted at 1 keV energy into 10 nm thick SiO_2 layers, which were thermally grown on (001) Si substrates. Using an AXCELIS GSD-ULTRA ultra-low-energy implanter, fluences of $5\times10^{15}\,cm^{-2}$, $1\times10^{16}\,cm^{-2}$, and $2\times10^{16}\,cm^{-2}$ were implanted at room temperature. Surface charging due to implantation was compensated by a Xe plasma electron flood gun. The implanted samples were cleaned using a piranha solution and furnace annealed for 30 min in N_2 at 950 °C. From all samples, cross sectional and plane view TEM specimens were prepared by the standard procedure of grinding, dimpling and Ar^+ ion beam thinning. PEELS-STEM was performed on plane view samples using a Scanning TEM VG-HB 501 operating at 100 kV that is equipped with a field emission cathode and a parallel Gatan 666 EELS spectrometer. Low-loss EELS spectra were recorded at each picture point, hence a spectrum image was acquired [8]. Using a non negative least square method [9], these spectra were fitted in the energy range of $15-30$ eV by a weighted sum of two plasmon reference spectra, which were obtained from bulk Si and SiO_2. Potential size-effects like shifts of the Si plasmon resonance of small Si NCs were not compensated. The gray level of the PEELS-STEM image pixels is given by the ratio of the intensity of the Si plasmon peak and the total intensity of the Si and SiO_2 plasmon peaks and, therefore, maps the Si bulk plasmons. Quantitative Si concentrations, however, can not be given, only the relative Si content is imaged. In Fig. 1, such Si plasmon maps (on the left hand side) are compared to plane view snapshots

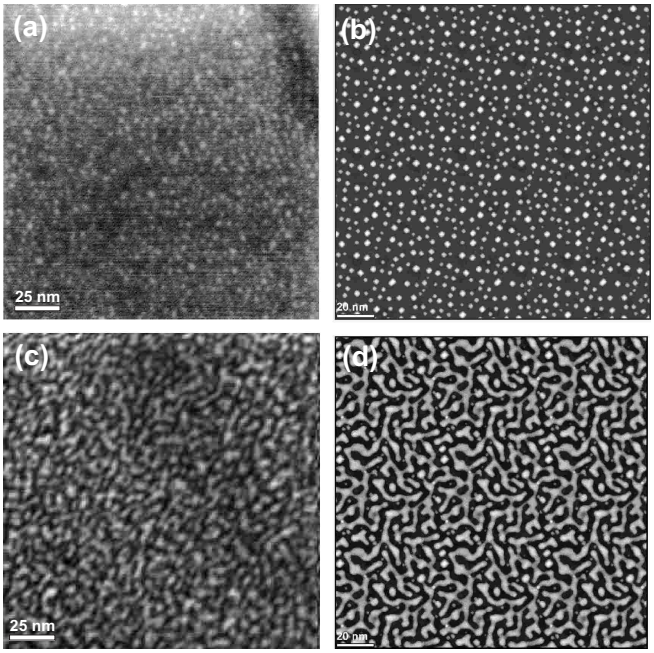

FIG. 1: Morphology of phase separated Si in SiO_2. Si plasmon maps by PEELS-STEM (a,c) are compared to corresponding KMC simulations (b,d). Nucleation of Si NCs is observed (a) for a Si fluence of $1\times10^{16}\,\mathrm{cm}^{-2}$ and predicted with the same morphology for (b) $3\times10^{15}\,\mathrm{cm}^{-2}$. Spinodal patterns are imaged (c) for $2\times10^{16}\,\mathrm{cm}^{-2}$ and simulated (d) for $8\times10^{15}\,\mathrm{cm}^{-2}$. White and black regions correspond to Si and SiO_2 phases, respectively.

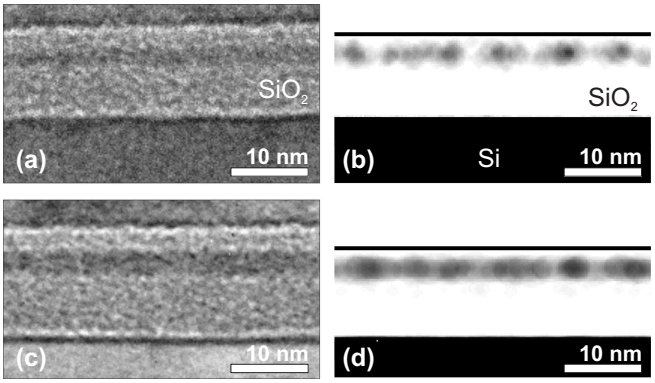

FIG. 2: Cross section view of the layer of phase separated Si in SiO_2. Fresnel XTEM images for (a) $1\times10^{16}\mathrm{Si}^{+}\,\mathrm{cm}^{-2}$ and (c) $2\times10^{16}\mathrm{Si}^{+}\,\mathrm{cm}^{-2}$ are compared to cross sectional KMC simulation snapshots for (b) $3\times10^{15}\mathrm{Si}^{+}\,\mathrm{cm}^{-2}$ and (d) $8\times10^{15}\mathrm{Si}^{+}\,\mathrm{cm}^{-2}$.

of kinetic Monte Carlo simulations (on the right hand side). This atomistic approach to phase separation of excess Si in thin SiO_2 layers by atomistic simulations was recently described in detail in Ref. [4] and [10]. The depth profiles of excess Si due to high fluence Si^+ ion implantation into thin gate oxides have been calculated by the binary collision program TRIDYN [11] accounting for the effects of ion erosion, target swelling and ion beam mixing dynamically. The post-implantation phase separation during thermal treatment is described by a kinetic 3D lattice Monte Carlo program package [12, 13]. Taking the TRIDYN profiles of Si excess as well as Si solubility and diffusivity in SiO_2 as input, the program describes excess Si diffusion, precipitation and Ostwald ripening in the thin SiO_2 layer under the constraints of the boundary conditions of a nearby Si/SiO_2 interface and a free SiO_2 surface. Here, we use a simplified version of the KMC program, i.e. only Ising-type nearest-neighbor interactions of diffusing Si atoms. It should be noted that KMC simulations with measured Si self-diffusivities [14, 15] lead to too long annealing times or too high temperatures. Obviously, the diffusive Si mass transport by a mobile SiO_2 defect with local Si excess (that could either be named Si interstitial, SiO molecule [14], or oxygen vacancy [16]) does not necessarily follow the same mechanism than as the $^{28}SiO_2/^{30}SiO_2$ interface broadening, which was analyzed in self-diffusivity studies. In this letter, the discrepancy between diffusive Si mass transport and Si self-diffusivity will not be discussed as our theoretical predictions aim at the reaction pathway of SiO_x decomposition rather than at a quantitative prediction of annealing time and temperature. Thus, KMC simulations utilize a relative time scale "Monte Carlo steps" (MCS) that allows a posterior recalibration with realistic Si diffusivities [13].

Subsequent image processing of KMC simulation data allowed to obtain KMC simulation snapshots (plane view or cross section) that can be compared directly to PEELS-STEM or Fresnel images. In plane view, the simulation cell has been tripled laterally taking advantage of the periodic boundary conditions. The number of excess Si atoms in the vertical column below the pixel at (x,y) determines the gray level of that pixel. The highest occurring number of Si atoms in such a column is assigned to white, whereas black means that no Si excess is found in the SiO_2 matrix. In plane view images, Si atoms of the underlying (001) Si substrate are not considered.

No Si precipitates were observed in the sample for the lowest Si^+ fluence of $5\times10^{15}\,\mathrm{cm}^{-2}$ (TEM images not shown here). For the medium Si^+ fluence of $1\times10^{16}\,\mathrm{cm}^{-2}$, white spots in a dark background appear in the plane view Si plasmon map shown in Fig. 1 (a) indicating spherical Si NCs embedded in the SiO_2 matrix. During thermal annealing, these NCs have formed by nucleation and growth in the Si enriched region of the implanted SiO_2 layer. The observed NCs are relatively small with an estimated mean diameter of 2.7 nm and have a high area density of $3.3\times10^{12}\,\mathrm{cm}^{-2}$. A similar precipitate morphology with the same mean NC size and density is found in the plane view KMC simulation snapshot of Fig. 1 (b), but for a significantly lower Si^+ fluence of $3\times10^{15}\,\mathrm{cm}^{-2}$ and a KMC simulation (annealing) time of 2100 kMCS. It should be noted that even this "medium" experimental Si^+ fluence of $1\times10^{16}\,\mathrm{cm}^{-2}$ leads in the KMC simulation to the formation of coalesced poly-Si layer buried in the SiO_2 [4]. For the highest Si^+ fluence of $2\times10^{16}\mathrm{Si}^{+}\,\mathrm{cm}^{-2}$, the morphology of the phases separated Si has changed completely as observed in Fig. 1 (c). A spaghetti-like network of white and black regions is found. This spinodal pattern clearly indicate that, at this fluence, phase separation took place by spinodal decomposition. Even more, percolation is observed. Si pre-

cipitates are no longer spatially isolated, but an interconnected network of phase separated Si has formed. An equivalent morphology with the same typical distances than in Fig. 1 (c) between the spinodal fingers is found in the plane view KMC simulation snapshot of Fig. 1 (d). This results was obtained for 8×10^{15} $Si^+ cm^{-2}$ and a simulation time of 300 kMCS. Strikingly, the morphology agrees remarkably well between both images, while simulation snapshots for other fluences or annealing times deviate instead considerably from the morphology seen in Fig. 1 (c).

Samples were studied additionally in cross section using a CM30 Phillips TEM equipped with a LaB_6 cathode operating at 300 kV. Fresnel imaging conditions were applied in order to achieve at least a weak contrast between Si and SiO_2 in cross sectional TEM (XTEM) images [5]. I.e. images were taken at Out-of-Bragg alignment and under strongly underfocused bright field conditions. Details of the responsible contrast mechanism are given in Ref. [5]. In Fig. 2, (a) and (c) show the XTEM Fresnel images for fluences of 1×10^{16} $Si^+ cm^{-2}$ and 2×10^{16} $Si^+ cm^{-2}$, respectively. Cross section KMC simulation snapshots are displayed in Fig. 2 (b) and (d) for 3×10^{15} $Si^+ cm^{-2}$ (2100 kMCS) and 8×10^{15} $Si^+ cm^{-2}$ (300 kMCS), respectively. Thereby, the same type of image processing was applied to KMC cross section views than to plane views. However, substrate atoms are considered here too and the gray scale of the KMC images has been inverted. White and black regions correspond to SiO_2 and Si phases, respectively. In all images, the phase separated Si forms a single, sharp layer seen as gray band in the SiO_2 that is well separated from the SiO_2/Si interface. Due to the extremely shallow Si excess profile obtained by low-energy Si^+ implantation, phase separation is quasi confined to two dimensions. For 1×10^{16} $Si^+ cm^{-2}$, Si precipitates align nicely in a thin layer, which is just a few nanometers thick, Fig. 2 (a). When the Si^+ fluences is increased to 2×10^{16} $Si^+ cm^{-2}$, the precipitate layer remains comparatively well localized in depth, Fig. 2 (c), although the Si morphology observed in plane view has changed completely, Fig. 1 (c). The total SiO_2 thickness is systematically smaller for the KMC simulations than for the corresponding Fresnel XTEM images. Nevertheless, the distance between the Si/SiO_2 interface and the phase separated Si agrees nicely for experiment and simulation.

The Si fluences in our KMC simulations where chosen in order to obtain morphologies of phase separated Si, which are similar to experimental ones. This adjustments of our simulation reveals a strong discrepancy between experimental and theoretical Si fluences. More Si than theoretically predicted has to be implanted. Not all Si that has nominally been implanted into the SiO_2 is available for phase separation. The reason for the missing Si excess might be twofold. (i) Recent Time of Flight Secondary Ion Mass Spectroscopy measurements on low-energy, low-fluence $^{30}Si^+$ as-implanted SiO_2 samples indicate that only a fraction of about $0.5 - 0.7$ of the nominal Si^+ fluence has been implanted into the SiO_2 [17]. (ii) It is known that (Si or Ge) NC formation in very thin SiO_2 films is extremely sensitive to humidity absorbed by the as-implanted (damaged) glass network [19] as well as to oxidants being present either in the annealing ambient [18]. Thus, a considerable amount of the implanted Si might become oxidized during annealing. This explains also why no NCs have been observed by TEM for the lowest Si^+ fluence of $5 \times 10^{15} cm^{-2}$. The implanted Si has been oxidized completely during the thermal annealing. At the same time, oxidation of the implanted Si leads to a volume expansion that increases the overall SiO_2 layer thickness [6]. This swelling of the SiO_2 due to Si oxidation can be seen in the XTEM images of Fig. 2 (a,c) if compared to the KMC simulation snapshots Fig. 2 (b,d), which just include the SiO_2 expansion due to the incorporated Si atoms [10]. Here, the KMC simulations do not account for oxidation and the swelling caused by it. To do so, a multi-component KMC approach (Si + O) is needed. Though samples have been annealed under fixed experimental conditions, the KMC simulation snapshots of corresponding Si patterns refer to different simulation times. Two reasons might be responsible for this discrepancy in the evolution speed. At first, the oxidation of a substantial part of implanted Si might influence the kinetics, and secondly, the Si bulk diffusion in SiO_2 might differ substantially from the Si diffusion at the Si/SiO_2 interface, which is assumed till now in the simulations. Studies that investigate this point are underway.

Summarizing, extensive studies on low-energy ion beam synthesis of multi-dot Si floating-gates embedded in thin SiO_2 layers have been presented. The morphology of this floating-gate layer formed by Si phase separation from SiO_2 has been revealed by Si plasmon mapping using PEELS-STEM. A direct comparison to kinetic 3D lattice Monte Carlo simulation snapshots have been made for the first time and shows a remarkable agreement between the atomistic simulations and the PEELS-STEM images. A strong fluence dependence of the precipitate morphology is confirmed. For low Si^+ fluences, isolated Si NCs form by nucleation and growth, while high fluences lead to spinodal decomposition during annealing and therefore to the formation of elongated precipitates, which additionally become percolated. With respect to a future applications in nonvolatile multi-dot floating-gate memories, structural percolation of the Si precipitates should be avoided. Otherwise, electrical charge brought to interconnected Si precipitates could spread easily in lateral dimension, i.e. the layer of phase separated Si would behave like a conventional poly-Si floating-gate. The present studies point out that, in order to prevent percolation, Si implantation (at 1 keV energy) should not exceed a limiting fluence of 1×10^{16} $Si^+ cm^{-2}$. Then, a thin layer of isolated, spherical Si NCs forms during annealing. However, the predicted fluence for spinodal pattern is lower than the experimental one. A substantial fraction of the implanted Si might be lost due to oxidation by oxidants penetrated from the ambient atmosphere.

This work was supported by the European Commission through the Growth project G5RD/2000/00320 – NEON (Nanoparticles for Electronics).

* Electronic address: T.Mueller@fz-rossendorf.de
† on leave from Ioffe Physico-Technical Institute, St. Petersburg

[1] S. Tiwari, F. Rana, H. Hanafi, A. Hartstein, E. F. Crabbe, and K. Chan, Appl. Phys. Lett. 68, 1377 (1996).
[2] S. Tiwari, J.A. Wahl, H. Silva, F. Rana, J.J. Welser, Appl. Phys. A 71 403 (2000).
[3] E. Kapetanakis, P. Normand, D. Tsoukalas, K. Beltsios, Appl. Phys. Lett. 80, 2794 (2002).
[4] T. Müller, K.-H. Heinig, and W. Möller, Appl. Phys. Lett. 81, 3049 (2002).
[5] G. B. Assayag, C. Bonafos, M. Carrada, P. Normand, D. Tsoukalas, and A. Claverie, Appl. Phys. Lett. 82, 200 (2003).
[6] M. Carrada, N. Cherkashin, C. Bonafos, G. Benassayag, D. Chassaing, P. Normand, D. Tsoukalas, V. Soncini, A. Claverie, Mat. Sci. & Eng. B 101 204 (2003).
[7] C. Bonafos, M. Carrada, N. Cherkashin, H. Coffin, D. Chassaing, G. Ben Assayag, A. Claverie, T. Müller, K. H. Heinig, M. Perego, M. Fanciulli, P. Normand, and D. Tsoukalas, J. Appl. Phys. 95, 5696 (2004).
[8] C. Jeanguillaume and C. Colliex, Ultramicroscopy 28, 252 (1989).
[9] C.L. Lawson, R.J. Hanson, Solving least square problems, Prentice-Hall, Englewood cliffs, New-Jersey, 1974.
[10] T. Müller, K.-H. Heinig, and W. Möller, Mat. Sci. & Eng. B 101/1-3, 49 (2003).
[11] W. Möller, W. Eckstein, Nucl Instr. & Meth. in Phys. Res. B 2 814 (1984).
[12] K.-H. Heinig, T. Müller, B. Schmidt, M. Strobel, W. Möller, Appl. Phys. A, 77 (2003) 17.
[13] M. Strobel, K.-H. Heinig, and W. Möller, Phys. Rev. B 64, 245422 (2001).
[14] M. Uematsu, H. Kageshima, Y. Takahashi, S. Fukatsu, K. M. Itoh, K. Shiraishi, and U. Gösele, Appl. Phys. Lett. 84, 876 (2004).
[15] D. Mathiot, J. P. Schunck, M. Perego, M. Fanciulli, P. Normand, C. Tsamis, and D. Tsoukalas, J. Appl. Phys. 94, 2136 (2003).
[16] J. Song, L. R. Corrales, G. Kresse, and H. Jonsson, Phys. Rev. B 64, 134102 (2001).
[17] M. Perego, M. Fanculli, G. Ben Assayag, A. Claverie, private communication (2003).
[18] S. Oswald, B. Schmidt, K.-H. Heinig, Surf. Interface Anal. 29, 249 (2000).
[19] B. Schmidt, D. Grambole, F. Herrmann, Nucl Instr. & Meth. in Phys. Res. B 191 482 (2002).